Journal of Analysis and Testing (2022) 6:353–364
https://doi.org/10.1007/s41664-022-00232-0

ORIGINAL PAPER

Development of a Handheld Nano-centrifugal Device for Visual Virus Detection

Zi-Rong Bi[1,2] · Meng-Lu Hu[2] · Yong-Zhong Jiang[3] · Er-Hu Xiong[2] · Bo-Wen Shu[4] · Si-Qi Li[6] · Han-Wei Chen[1,5] · Xiao-Hua Chen[1,7] · Xiao-Ming Zhou[2]

Received: 10 March 2022 / Accepted: 12 May 2022 / Published online: 5 August 2022

Abstract

Gold nanoparticles (AuNPs) colorimetric assays based on distance-dependent optical characteristics have been widely employed for bioanalysis. However, this assay is not effective for visually detecting low-concentration targets due to the faint color change. Here, we developed a handheld nano-centrifugal device which could separate the crosslinked and non-crosslinked AuNPs. Results showed that the handheld nano-centrifugal device could easily reach more than 6000 r/min within 10 s simply by stretching and tightening the coiled rope in an appropriate rhythm. Further, combined with the CRISPR/Cas12a nucleic acids recognition system, a field-deployable colorimetric platform termed handheld nano-centrifugal device assisted CRISPR/Cas12a (Hand-CRISPR) has been validated. Moreover, clinical diagnostics applications for Epstein-Barr virus (EBV) and severe acute respiratory syndrome coronavirus-2 (SARS-CoV-2) detection with high sensitivity and accuracy (100% consistency with reverse transcription quantitative real-time polymerase chain reaction (RT-qPCR) test results) have been demonstrated. Overall, the Hand-CRISPR platform showed great promise in point-of-care-test (POCT) application, expected to become a powerful supplement to the standard nucleic acid testing method in remote or poverty-stricken areas.

Keywords Nucleic acids assay · CRISPR/Cas12a · Gold nanoparticles · Centrifugal device · Clinical diagnostics

✉ Han-Wei Chen
docterwei@sina.com

✉ Xiao-Hua Chen
cxh0663@126.com

✉ Xiao-Ming Zhou
zhouxm@scnu.edu.cn

1 South China Normal University-Panyu Central Hospital Joint Laboratory of Basic and Translational Medical Research, Guangzhou Panyu Central Hospital, Guangzhou 511400, China

2 School of Life Sciences, South China Normal University, Guangzhou 510631, China

3 Hubei Provincial Center for Disease Control and Prevention, Wuhan 430079, China

4 Dermatology Hospital, Southern Medical University, Guangzhou 510091, China

5 Medical Imaging Institute of Panyu, Guangzhou 511400, China

6 Department of Ultrasound, Panyu Central Hospital, Guangzhou 511400, China

7 Cancer Center, Integrated Hospital of Traditional Chinese Medicine, Southern Medical University, Guangzhou 510315, China

1 Introduction

Rapid, accurate and sensitive nucleic acid detection has been considered as one of the most important tools in clinical diagnosis, biomedical research, environmental monitoring, food safety, and so on [1–6]. Due to its high sensitivity and specificity, polymerase chain reaction (PCR) is the gold-standard technique for nucleic acid detection. However, it still has some drawbacks, such as long turnaround time, reliance on sophisticated equipment, central lab, and skilled technicians. These shortcomings are likely to hinder its widespread application, especially in places where medical resources and infrastructure are scarce. Therefore, it is of great significance to develop a point-of-care (POC) molecular diagnostic platform suitable for non-laboratory environments [7].

As an easy and cost-effective alternative in the field of POC testing, gold nanoparticles (AuNPs)-based colorimetric assays have attracted considerable research interest because they can transform molecular recognition events into color changes, which can avoid the complexity in optical or electrical detection methodologies. Due to the unique

distance-dependent optical properties of the AuNPs, the colorimetric assay based on AuNPs can be distinguished by naked eyes [8]. More recently, researchers have coupled this typical colorimetric assay with the clustered regularly interspaced short palindromic repeats (CRISPR)/Cas system, which not only enhanced the probes universality but also greatly improved the sensitivity of molecular detection [9–11]. Although similar assays have been widely used in the field of nucleic acid detection since its development, a common problem is often encountered in practical applications: when detecting low-concentration targets, only a small number of AuNPs are crosslinked and aggregated, while most AuNPs are dispersed. Under such situation, the color of the AuNPs solution only slightly changed, which will lead to a low signal-to-noise ratio. Thus, separation of the crosslinked and non-crosslinked AuNPs-DNA probes may be a solution for this issue. Since the majority of crosslinked AuNPs will form a network-like complex, high-speed centrifugation is a relatively more straightforward and effective way to separate the dispersed and the crosslinked AuNPs-DNA probes. Although the commercial benchtop centrifuge has been proven effective in precipitating the crosslinked AuNPs [10], its application in POC diagnostics scenarios is limited because of its inconvenience and requirement for a power supply.

To address the above issues, it is useful to develop simple and portable tools without an additional power supply, and the rotational speed can be comparable to a high-speed commercial centrifuge. To enable bio-separation in non-laboratory settings, the researchers have developed a series of human-powered centrifugal platforms for centrifugation such as egg-beaters [12], salad-spinners [13], buzzer toys [14, 15], and fidget-spinners [16, 17]. Most of these tools were successfully applied in the fields of low-speed bio-separation, such as blood plasma separation and nucleic acid extraction [12, 15]. However, to date, with the help of a fully human-powered centrifugal device, it remains unknown whether it is possible to achieve high-speed separation of nano-scale materials.

In this study, inspired by an ancient spinning device-the buzzer, we engineered a fully human-powered nano-centrifugal device for conveniently and visually detecting nucleic acids. This handheld nano-centrifugal device is an electricity-free platform that can effectively transfer manual operation into high-speed rotations. Based on the theoretical analysis and experimental results, we demonstrated that this device can effectively separate the crosslinked and non-crosslinked AuNPs-DNA probes in just 10–20 s, thereby obtaining colorimetric results with a high signal-to-noise ratio. Furthermore, by successfully combining the handheld nano-centrifugal device with the CRISPR/Cas12a system (Hand-CRISPR), we developed a low-cost, palm-sized, and highly reliable platform for visual virus detection. Using this platform, we successfully demonstrated its utility for accurate and convenient detection of Epstein-Barr virus (EBV) and severe acute respiratory syndrome coronavirus-2 (SARS-CoV-2). Overall, the Hand-CRISPR we developed is a rapid, low-cost, reliable platform without an external power supply, which shows great promise in POC application, and becomes a powerful supplement to the gold-standard method in remote or poverty-stricken areas.

2 Material and Methods

2.1 Handheld Nano-Centrifugal Device-Assisted the CRISPR/Cas12a-Mediated Colorimetric (Hand-CRISPR) Assay

Cas12a/crRNA reaction buffer: 10 mmol/L Tris–HCl (pH 9.0), 10 mmol/L NaCl, 15 mmol/L $MgCl_2$, 5% PEG-200. A 20 μL reaction cocktail contained 100 nmol/L LbCas12a, 200 nmol/L linker ssDNA substrate, and 500 nmol/L crRNA. DNA amplified product (2 μL) was added to the cocktail and reacted for 20 min. After that, 60 μL of AuNPs-DNA probes premixed solutions (30 μL of AuNPs-DNA probe 1 and 30 μL of AuNPs-DNA probe 2) were added to the reaction solution. The cocktails were incubated at room temperature for 3 min and centrifuged with the handheld nano-centrifugal device for 10–20 s. The supernatant was used for direct visualization or UV–vis analysis.

For additional experimental details, please refer to the Supporting Information.

3 Results and Discussion

3.1 Scheme of the Design of Centrifugation Based Colorimetric Assay

DNA functionalized AuNPs can hybridize with ssDNA (linker) to form a network-like crosslinked complex, inducing a distinct color change (from red to purple). But in the actual detection application, the following three situations will be encountered: (i) AuNPs are completely dispersed and the solution remains red (in the absence of linker-ssDNA); (ii) AuNPs are completely aggregated and the solution color turns purple (high concentration of linker-ssDNA); (iii) AuNPs are partially aggregated and this is a critical situation (low concentration of linker-ssDNA). When AuNPs are partially aggregated, only faint color change can be observed, making it difficult to judge the detection results by the naked eye.

To address this issue, here we aim to develop a handheld nano-centrifugal device, which could effectively separate the crosslinked AuNPs-DNA probes from the AuNPs-DNA

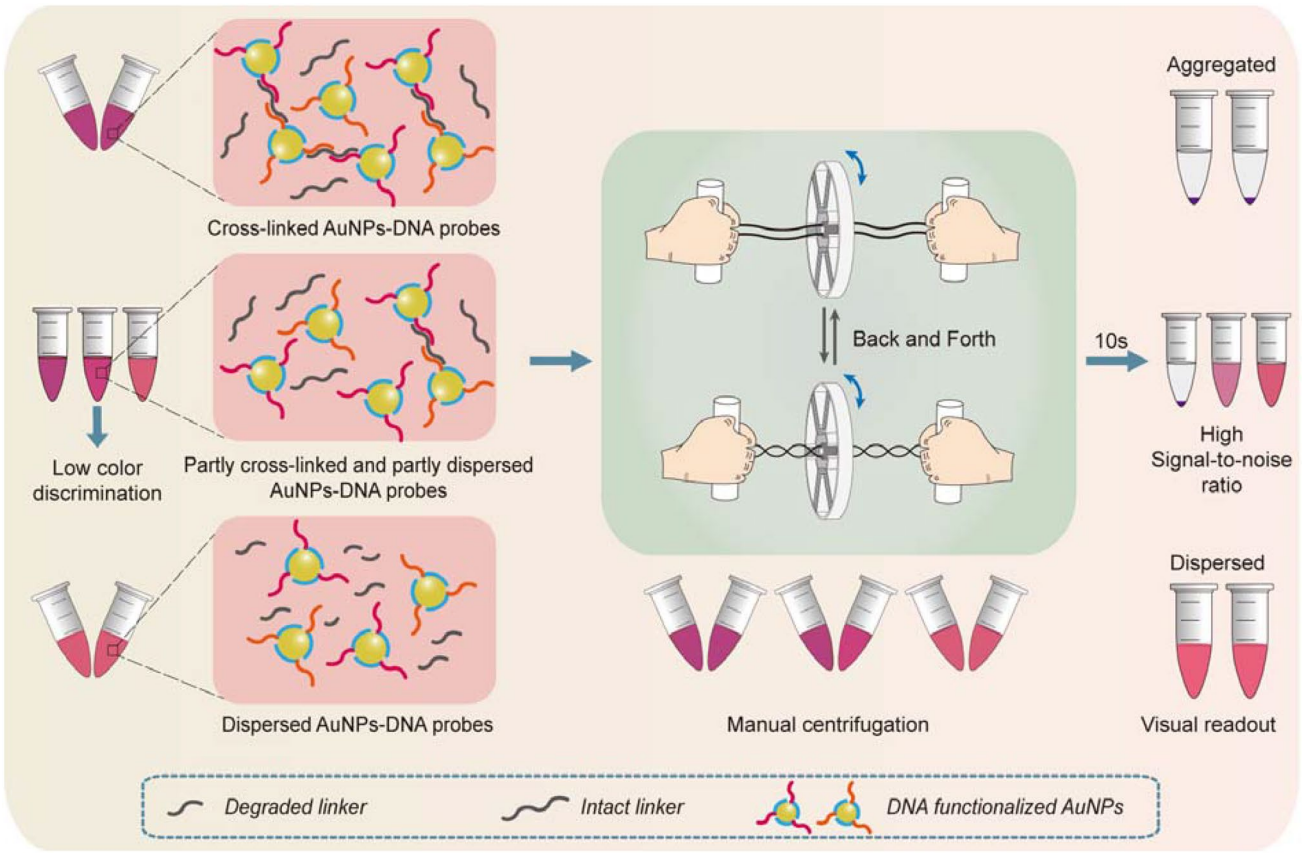

Scheme 1 The design of centrifugation-based colorimetric assay

monomer via high-speed centrifugation. As shown in scheme 1, we first designed a pair of universal AuNPs-DNA probes, which could hybridize with ssDNA linker and produce crosslinked aggregates. After adding the ssDNA linker to equal volumes of two premixed AuNPs-DNA probes solutions, the crosslinked AuNPs aggregates would be effectively precipitated to the bottom of the tube by rhythmical pulling the ropes of the handheld nano-centrifugal device. Thus, with the help of a handheld nano-centrifugal device, we hope to realize a colorimetric detection method which is more convenient for visual observation.

3.2 Handheld Nano-centrifugal Device

The handheld nano-centrifugal device used in this study is specifically composed of three parts: a 3D-printed centrifugal disc, a nylon rope, and two 3D-printed handles, as shown in Fig. 1a. This handheld nano-centrifugal device is capable of holding and effectively spinning down six samples of PCR tubes (with a capacity of 0.2 mL) simultaneously without resorting to an external power supply, and the manufacturing cost is extremely low (< 20 cents). Furthermore, each chamber on the centrifugal disc was designed as three-quarters of the hollow cylinder. On one hand, it could fix the PCR tube. On the other hand, the operator could directly observe the color inside the PCR tube without removing it from the device. Then, a nylon rope was used to pass through two symmetrical holes in the center of the disc, and each end of the rope was tied around a handle. After the PCR tubes were firmly clamped at the chamber on the centrifugal disc, the tape could additionally be used to ensure that the PCR tubes would not become loose.

The schematic diagram of manual centrifugal operation is shown in Fig. 1b. We coil the rope in a supercoiled state and then apply outward tension to accelerate the centrifugal disc to the maximum rotational speed. When the rope is close to unwinding, the inertia of the centrifugal disc will drive the rope to rewind. By repeating the above cycle, the centrifugal disc could quickly reach to the maximum rotational speed.

3.3 Validation of the Handheld Nano-centrifugal Device

A high-speed benchtop centrifuge experiment was first executed to determine the lowest centrifugal speed capable of effectively separating the monodisperse and aggregated

AuNPs in a short time. Thus, a 30 s centrifugation experiment was performed with an increment of 1000 r/min per time. Based on the color intensity and the UV–vis absorbance measurement, the minimum rotational speed was finally determined to be 6000 r/min (Fig. 1c). To guide the design of a 3D-printed centrifugal disc (Fig. 1d), it is needed to calculate the mean input force (F_m) required by the operator when the handheld centrifugal disc reaches the maximum angular velocity ($\dot{\phi}_{max} = 6000$ r/min). We assume a weightless and inextensible rope with evenly tension distribution. Meanwhile, we only consider the constant input force. The relationship between the total torque (M) and the angular acceleration ($\ddot{\phi}$) can be expressed as:

$$M = I \times \ddot{\phi} \tag{1}$$

where I is the inertial moment of the disc, $I = m \times {R_d}^2$, m is the mass of the centrifugal disc, R_d is the radius of the centrifugal disc.

To find the relationship between $\dot{\phi}_{max}$ and F_m, we assume that the ropes on both sides of the 3D-printed centrifugal disc are in the state of zero-twist point reported by Bohr and Olsen [18], that is the state where the rope cannot be further twisted without compression or forming of a supercoiling structure. Prakash et al. defined the angular displacement of the handheld centrifugal disc in this state as ϕ_{crit} and based on this study [14], the maximum angular velocity can be written as:

$$\dot{\phi}_{max} = \phi_{crit} \times \omega = \frac{L \times \sqrt{\pi^2 - 2^2}}{2R_s} \bullet \sqrt{\frac{2F_m \times R_s^2}{I \times L}}, \tag{2}$$

So, we can write the relationship between $\dot{\phi}_{max}$ and F_m simply as:

$$F_m = \frac{2{\dot{\phi}_{max}}^2 \times m \times R_d^2}{L \times \left(\pi^2 - 2^2\right)}, \tag{3}$$

where R_s is the radius of the circular cross section of the rope, L is the distance between handle and the centrifugal disc.

According to Eq. 3, we can see that F_m is related to R_d, L, m and $\dot{\phi}_{max}$.

First, we designed three different sizes of centrifugal discs, and the corresponding parameters were shown in Table S1. Then, we calculated the mean input force required for these three sizes of centrifugal discs to reach 6000 r/min according to the parameters in Table S1. Finally, we calculated that the mean input force $\left(F_m\right)$ required for the centrifugal disc with a radius of 3 cm, 4.5 cm, and 6 cm to reach 6000 r/min were 6.3 N, 23.7 N, and 63.8 N, respectively. It can be concluded that the No.1 design of the centrifugal disc has a smaller mass, and the operators only need less effort to obtain the maximum rotational speed.

In addition to theoretically calculating the mean input force, we also performed a test on the above three sizes of handheld centrifugal discs by validating their separation performance of the monodisperse and aggregated AuNPs, and the results were shown in Fig. 1e. In the case of ensuring the concentration of ssDNA linker was saturated (Fig. S1), only the No. 3 design of the centrifugal disc could not effectively separate the crosslinked AuNPs to the bottom of the tube. The remaining two sizes of centrifugal discs were able to obtain the colorless supernatant within 60 s. After taking into account the separation result of the crosslinked AuNPs and other parameters such as the mass, cost and F_m of the centrifugal disc (Table S1), we finally selected the centrifugal disc with a radius of 3 cm for subsequent experiments (Fig. S2).

3.4 Construction of a High-Efficient AuNP Colorimetric System

According to the formula of centrifugal force, there is a positive correlation between the mass of the object and the centrifugal force. Therefore, we considered that variation of the diameter of AuNPs may exhibit different centrifugation performance of crosslinked AuNPs. We used the sodium citrate reduction method to prepare AuNPs with diameter in 20 nm and 13 nm for comparative analysis (Fig. S3). Both AuNPs were functionalized DNA by freeze-based labeling methods, as previously reported by our group [19]. Next, we aimed to determine the critical concentration of ssDNA linker that could cause the full crosslinking of AuNPs-DNA probes (13 nm, 20 nm, respectively). In this experiment, we used varied ssDNA linker concentrations (0, 10, 20, 30, 40 and 50 nmol/L) to test the crosslinking behavior of two different-sized AuNPs-DNA probe pair (5 nmol/L). After high-speed centrifugation through the handheld nano-centrifugation device, a colorless supernatant and low UV–vis absorbance at 520 nm indicated that the crosslinking reaction was saturated when the concentrations of ssDNA linker were higher than 20 nmol/L for the 20 nm AuNPs. However, for the 13 nm AuNPs, the ssDNA linker concentrations needed to be higher than 40 nmol/L to obtain a sufficient clean background (Fig. 2a). Further, we tested the shortest centrifugation time required for fully separating the crosslinked AuNPs-DNA probes using the handheld nano-centrifugal device. By direct observation and the UV–vis measurement (A_{520}/A_{650} and A_{530}/A_{650}), it was found that the 20 nm AuNPs crosslinked aggregates could be sufficiently separated in only 10 s. By contrast, it took about 30 s to fully separate the 13 nm AuNPs crosslinked aggregates (Fig. 2b and Fig. S4).

We next evaluated the hybridization performance of AuNPs-DNA probes prepared by a poly (*A*) affinity labeling method. According to the research of Fan

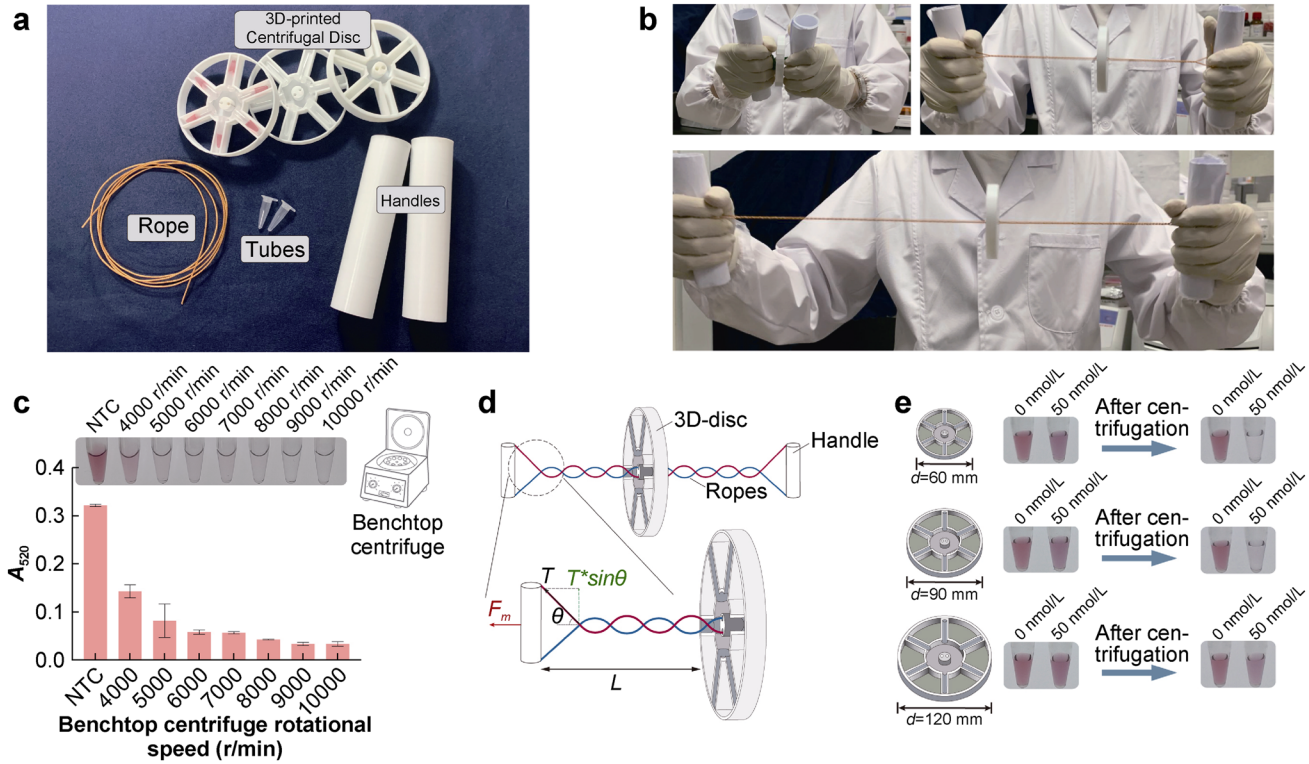

Fig. 1 Validation of the handheld nano-centrifugal device. **a** Materials used to construct the handheld nano-centrifugal device. **b** Images of manual centrifugal operation. **c** Separation result of crosslinked AuNPs by benchtop centrifuge at different rotational speeds. **d** Schematic diagram of a physical model of the handheld nano-centrifugal device. **e** Separation performance of the handheld nano-centrifugal device with a different radius on crosslinked AuNPs within 60 s. (In the experiments shown in **c** and **e**, the size of AuNPs is 13 nm. Data are represented as mean ± standard error of the difference between means of three technical replicates)

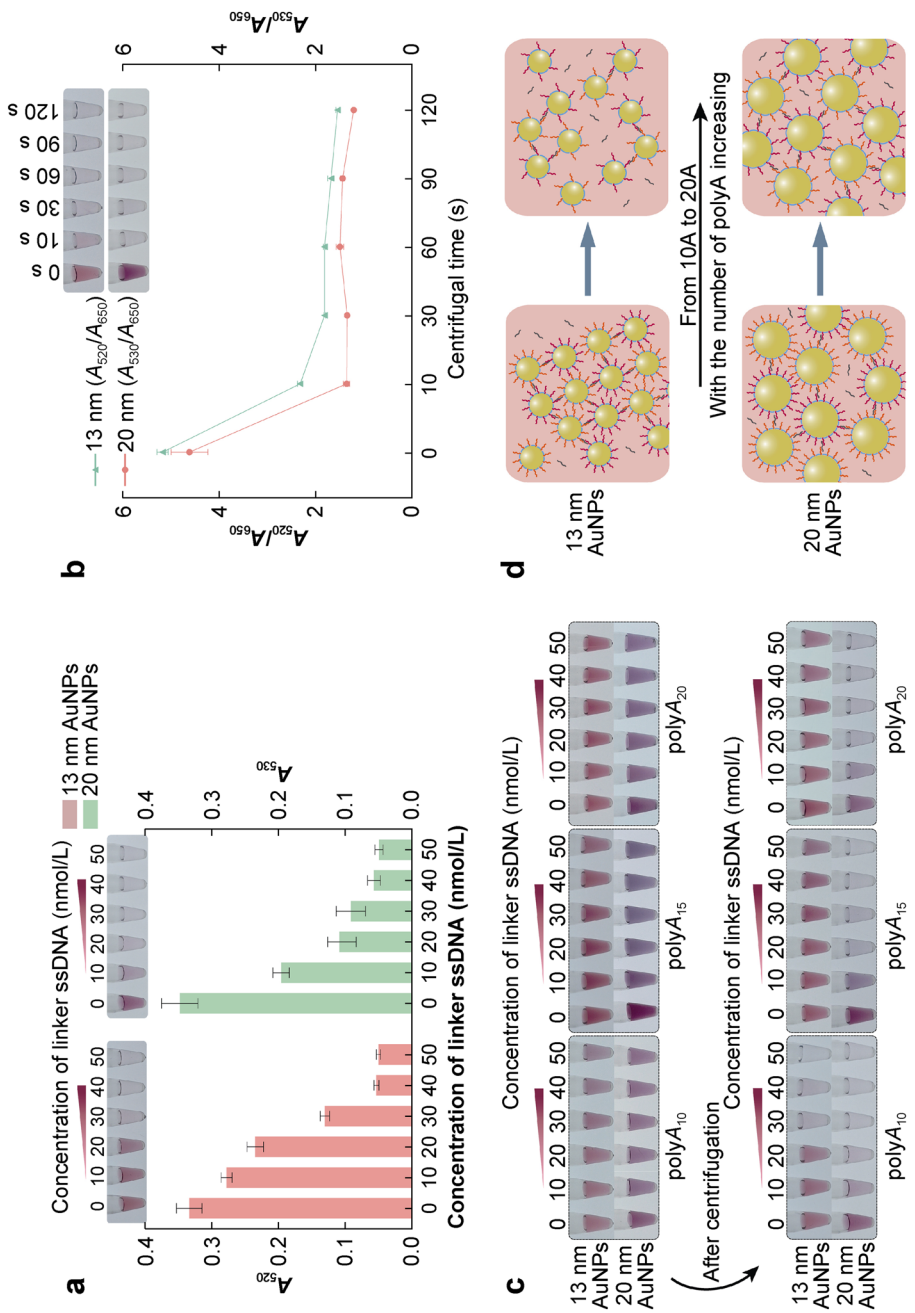

Fig. 2 Construction of a high-efficient AuNP colorimetric system by handheld nano-centrifugal device. **a** The crosslinking behavior of two different-sized AuNPs under different concentrations of ssDNA linker. **b** Screening of the shortest centrifugal time required for a handheld nano-centrifugal device to separate two different-sized AuNPs crosslinked aggregates. **c** Evaluation of the crosslinking behavior of two different-sized AuNPs before and after centrifugation with the increasing number of poly (*A*) for affinity labeling. **d** Schematic diagram of two different-sized AuNPs crosslinking behavior when increasing the number of poly (*A*) for affinity labeling. (Data are represented as mean ± standard error of the difference between means of three technical replicates)

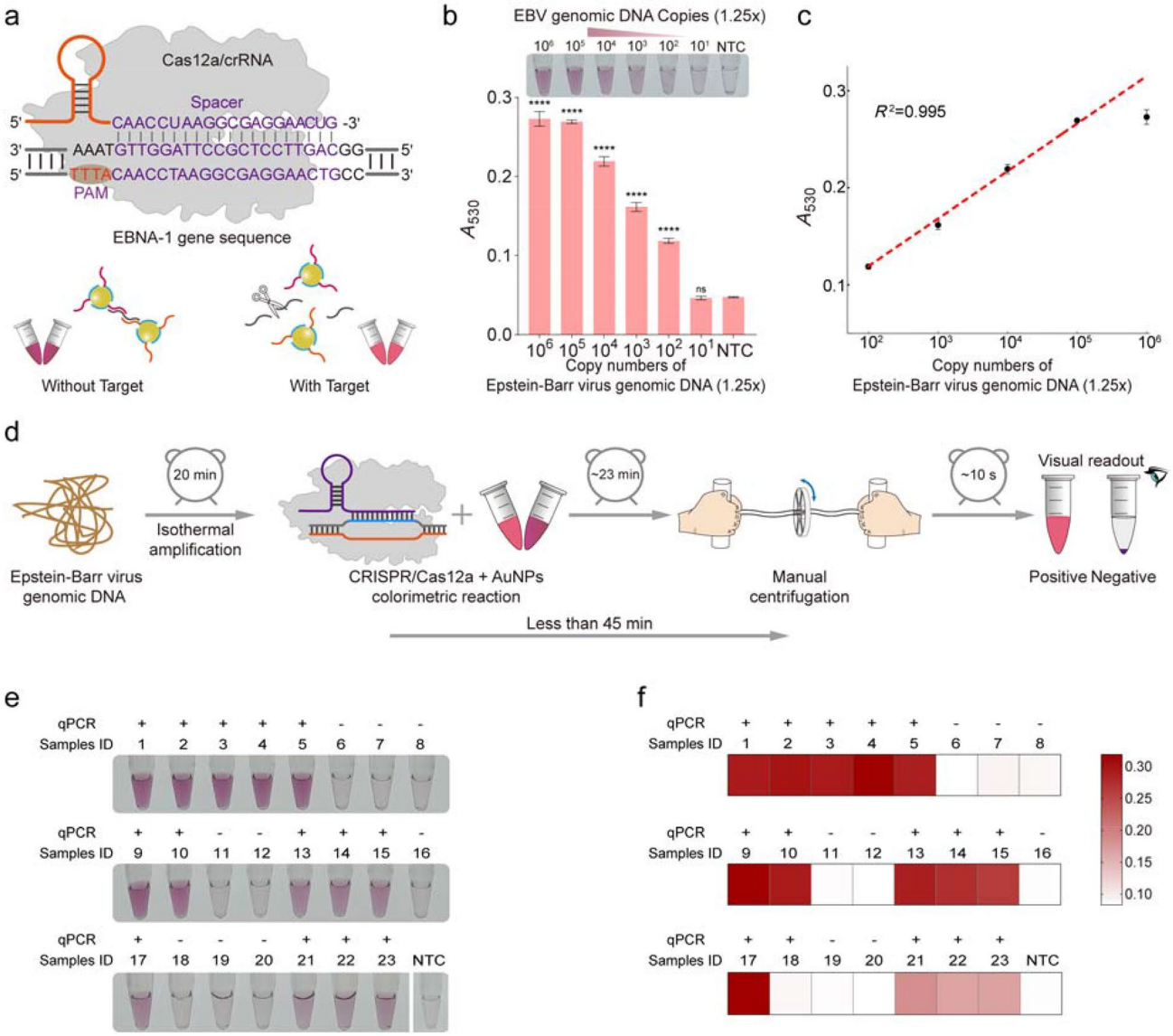

Fig. 3 Detection of Epstein-Barr virus by the Hand-CRISPR platform. **a** Schematic diagram of EBNA-1 gene sequence in EB virus recognized by Cas12a/crRNA system followed by colorimetric analysis. **b** Colorimetric analysis of RPA products using a tenfold serial dilution of EBV genomic samples. ($n=3$ technical replicates, two-tailed Student's test; ns, not significant; $^{**}p<0.01$; $^{***}p<0.001$; and $^{****}p<0.0001$; error bars represent three different individual experiments. NTC represents no-template control). **c** A linear relationship between the UV–vis absorbance (A_{530}) and the concentration of EBV genomic DNA. Data are represented as mean ± standard error of the difference between means of three technical replicates. **d** Schematic workflow of the Hand-CRISPR platform applied to rapid detection of EB virus. **e** The naked-eye detection of EBV positive samples by the Hand-CRISPR platform. **f** Heat map analysis based on the UV–vis spectrum results. Assessment of clinical sample detection ($n=23$). The "+" and "−" represent positive and negative samples, respectively, as confirmed by qPCR

et al. [20], with the increase of the number of poly (*A*), the number of oligonucleotides labeled on the surface of AuNPs will decrease, resulting in the reduction of steric hindrance and the improvement of probe hybridization efficiency on the surface of AuNPs. Therefore, we hypothesized that increasing poly (*A*) within a specific range (A_{10}–A_{20}) could improve the crosslinking reaction efficiency between AuNPs-DNA probes. However, for the 13 nm AuNPs, when the number of poly (*A*) increased, the solution color and UV–vis spectrum peak varied only slightly, although the ssDNA linker concentration for hybridization was saturated (50 nmol/L). The solution color remained unchanged after high-speed centrifugation with a handheld nano-centrifugal device. By contrast, under the same conditions, the solution color and UV–vis spectrum peak changed greatly with the help of a handheld nano-centrifugal device for the 20 nm AuNPs (Fig. 2c and Fig. S5).

Given the above phenomenon, we speculated that the steric hindrance of DNA probes on the surface of AuNPs would decrease as the length of poly (*A*) increasing, and the number of DNA probes labeled on the surface of AuNPs for hybridization would lessen at the same time (Fig. 2d). Compared with the improvement of DNA hybridization efficiency on the surface of AuNPs, the reduction of DNA probes on the surface of AuNPs has a more significant impact on the growth in size of the network-like crosslinked complex. Therefore, the change of solution color and UV–vis spectrum of the 13 nm AuNPs cannot be observed with poly (*A*) increasing. For the 20 nm AuNPs, because the number of DNA probes labeled on its surface are saturated for hybridization, increasing the number of poly (*A*) would reduce the steric hindrance on its surface and significantly improve the crosslinking reaction efficiency. In this way, the size of the network-like crosslinked complex would become larger at a certain incubation time, which was more conducive to separate the crosslinked AuNPs-DNA probes and the AuNPs-DNA monomer through a handheld nano-centrifugal device.

Next, we determined the above inferences by measuring the size distribution of hydrated particle size of crosslinked AuNPs aggregates, as shown in Fig. S6. First, we used the same concentration (50 nmol/L) of ssDNA linker and then incubated them for 3 min to test the hydrated particle size. The results showed that for the 13 nm AuNPs with poly (A_{10}) sequence, the particle size of the network-like crosslinked complex is generally in the range of 100–1000 nm, and a certain proportion is in the range of 4000–6000 nm. When the labeling sequence increased from poly (A_{10}) to poly (A_{20}), the crosslinked AuNPs aggregates with a particle size greater than 500 nm decreased significantly, but the proportion locating at 350 nm increased. On the contrary, for the 20 nm AuNPs, the particle size of the network-like crosslinked complex increased with the augment of the number of poly (*A*) bases. According to the experimental results, the larger the particle size of the crosslinked AuNPs aggregates, the easier it is to be precipitated by the handheld nano-centrifugal device. Therefore, we finally selected the 20 nm AuNPs with labeling sequence poly (A_{15}) for subsequent detection application.

3.5 Epstein-Barr Virus Detection by the Hand-CRISPR Platform

Epstein-Barr virus (EBV) is a kind of human herpesvirus, listed as a class I carcinogen by the international agency for research on cancer [21–23]. The EBV DNA in human serum is a useful research and clinical biomarker for nasopharyngeal carcinoma and other EBV-related diseases [24–27]. In this part, we combined the colorimetry method based on the handheld nano-centrifugal device with CRISPR/Cas12a system to detect the EBNA-1 gene in EBV DNA. The detection principle is shown in Fig. 3a. The designed Cas12a/crRNA complex recognizes a 20 bp target sequence in the conserved region (Epstein Barr virus nuclear antigen 1) EBNA-1 gene sequence adjacent to a TTTA protospacer adjacent motif (PAM) site. Then, the *trans*-cleavage activity is activated, and the universal ssDNA linker will be degraded nonspecifically. Therefore, in the presence of target DNA, the AuNPs-DNA probes are dispersed in solution remaining red. On the contrary, in the absence of target DNA, ssDNA linker is intact, and the AuNPs-DNA probes will form aggregates by crosslinking reaction. With the aid of a handheld nano-centrifugal device, we can identify the detection result by direct observation of the color change.

The EBV DNA genome sample was extracted from the human serum and then amplified with recombinase polymerase amplification (RPA) (20 min). We first used the amplified products of the EBNA-1 gene as targets to evaluate the sensitivity of the Hand-CRISPR platform. The results were determined by direct naked-eye observation or UV–vis analysis. As shown in Fig. 3b, the detection limit obtained by RPA was as low as approximately 125 copies of the genome sample without optimized amplification parameters. At the same time, a linear relationship ($R^2 = 0.995$) was obtained between the UV–vis absorbance (A_{530}) and the concentration of EBV genomic DNA over the range from 10^2 to 10^5 copies (Fig. 3c). Next, by calculating the time spent in the entire workflow of the rapid on-site detection, we have concluded that the Hand-CRISPR platform could complete an EBV DNA detection within 45 min (Fig. 3d). Subsequently, we assessed the actual utility of our developed platform using 23 human serum clinical samples, which were previously diagnosed using a qPCR method. The results based on direct observation and heat map analysis (Fig. 3e and f) showed 100% consistent with the quantitative polymerase chain reaction (qPCR) results (Fig. S7). These results indicate that our Hand-CRISPR platform has great application potential in POCT scenarios.

Fig. 4 Detection of SARS-CoV-2 by the Hand-CRISPR platform. **a** Schematic diagram of the full-length SARS-CoV-2 genome and the amplified region of Orf1ab gene (from 14,019 to 14,200) and N gene (from 29,099 to 29,275). **b** and **c** Sensitivity analyses of the Orf1ab gene and N gene, respectively. **d** Specificity analysis of the Hand-CRISPR platform for SARS-CoV-2 and other viruses. ($n = 3$ technical replicates, two-tailed Student's test; *ns*, not significant; **, $p < 0.01$; ***, $p < 0.001$; and ****, $p < 0.0001$; error bars represent three different individual experiments. NTC represents no-template control). **e** Schematic workflow of the Hand-CRISPR platform applied to rapid detection of SARS-CoV-2. **f** Assessment of clinical sample detection ($n = 20$). The heat map represents the values of the UV–vis spectra results. The "+" and "−" represent positive and negative samples, respectively, as confirmed by RT-qPCR

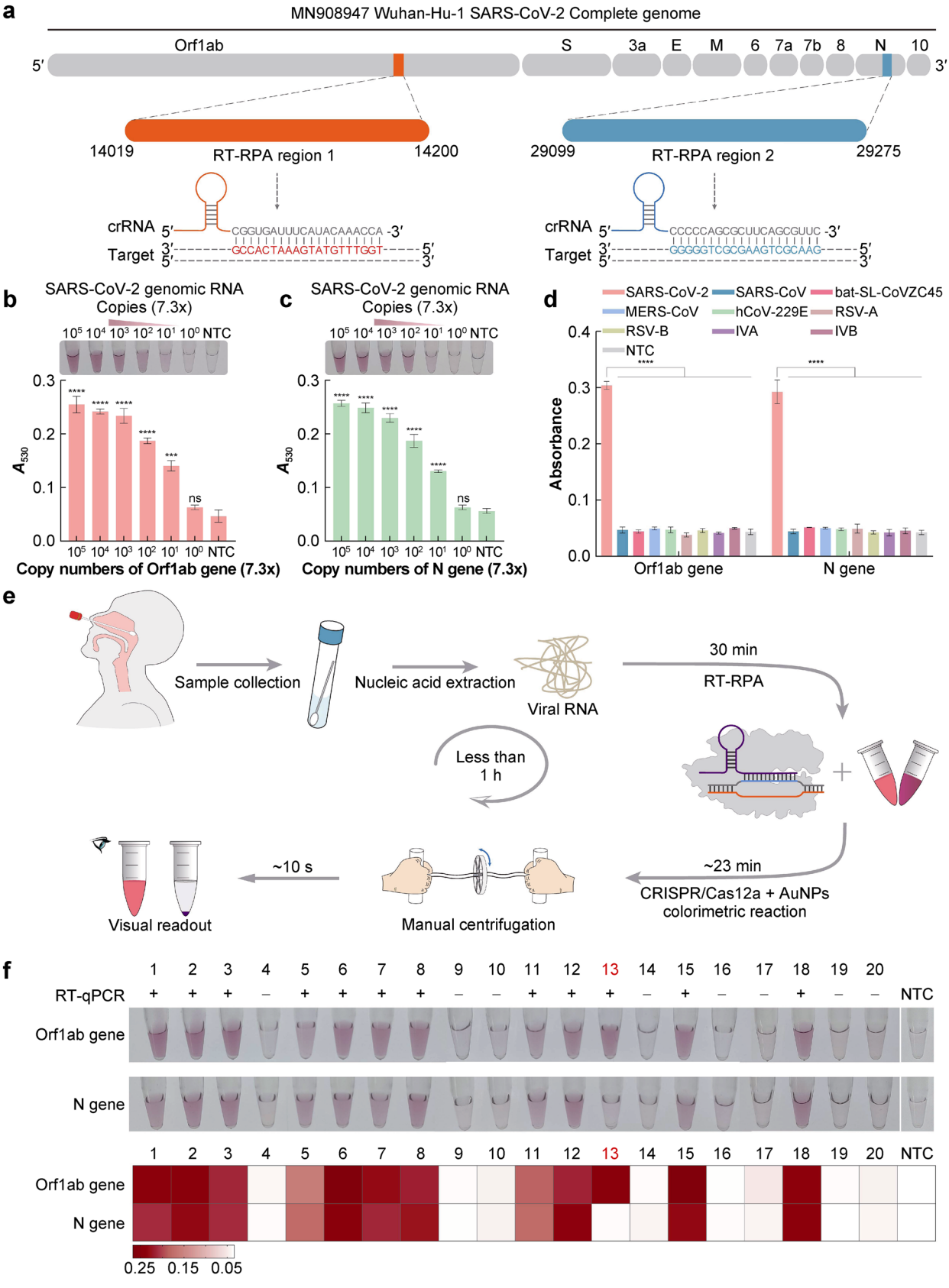
a
MN908947 Wuhan-Hu-1 SARS-CoV-2 Complete genome
Orf1ab
S
3a
E
M
6
7a
7b
8
N
10
5′
3′
14019
RT-RPA region 1
14200
29099
RT-RPA region 2
29275
crRNA 5′ CGGUGAUUUCAUACAAACCA -3′
Target 3′ GCCACTAAAGTATGTTTGGT 5′
crRNA 5′ CCCCCAGCGCUUCAGCGUUC -3′
Target 3′ GGGGGTCGCGAAGTCGCAAG 5′
b
SARS-CoV-2 genomic RNA Copies (7.3x)
10⁵ 10⁴ 10³ 10² 10¹ 10⁰ NTC
A530
Copy numbers of Orf1ab gene (7.3x)
c
SARS-CoV-2 genomic RNA Copies (7.3x)
Copy numbers of N gene (7.3x)
d
SARS-CoV-2
SARS-CoV
bat-SL-CoVZC45
MERS-CoV
hCoV-229E
RSV-A
RSV-B
IVA
IVB
NTC
Absorbance
Orf1ab gene
N gene
e
Sample collection
Nucleic acid extraction
Viral RNA
30 min
RT-RPA
Less than 1 h
~23 min
CRISPR/Cas12a + AuNPs colorimetric reaction
Manual centrifugation
~10 s
Visual readout
f
RT-qPCR
Orf1ab gene
N gene
NTC
0.25 0.15 0.05

3.6 SARS-CoV-2 Detection by the Hand-CRISPR Platform

SARS-CoV-2 RNA detection is the key measure for effective control of its widespread transmission [28–34]. Here, we aim to apply the low-cost, rapid and reliable Hand-CRISPR platform to the rapid detection of SARS-CoV-2 RNA, which is expected to be used as a screening platform for SARS-CoV-2 in remote or poverty-stricken areas. SARS-CoV-2 is an enveloped positive-sense RNA virus with a full-length RNA genome of nearly 30,000 nucleotides (nt) [35, 36]. In this part, we selected the open reading frame 1ab (Orf1ab) gene and nucleocapsid (N) gene as the target genes for detecting SARS-CoV-2 [31, 37]. Further, we evaluated the detection performance of the Hand-CRISPR platform from the aspects of sensitivity, specificity and actual utility.

As shown in Fig. 4a, the amplified regions ranged from 14,019 to 14,200 for Orf1ab gene, and from 29,099 to 29,275 for N gene were designed. The corresponding crRNAs were designed to target two different amplified regions, respectively, thus activating the *trans*-cleavage of the ssDNA linker near the CRISPR/Cas12a system nonspecifically. We first evaluated the analytical sensitivity of the Hand-CRISPR platform by targeting the in vitro transcribed RNA of Orf1ab and N genes which had been quantified by droplet digital PCR. After the real-time reverse transcription-polymerase chain reaction (RT-RPA) reactions, the Orf1ab and N genes amplicons were subjected to the CRISPR/Cas12a recognition, and the experimental results could be obtained by the naked-eye observation or UV–vis analysis. We could identify a limit of detection (LOD) of 73 copies per reaction (20 μL) for both Orf1ab and N genes (Fig. 4b and Fig. 4c). In addition, we further analyzed the specificity of the proposed Hand-CRISPR platform. Only RT-RPA test showed that SARS-CoV-2, bat coronavirus RaTG13 (bat-SL-CoVZC45), and severe acute respiratory syndrome virus (SARS-CoV) could not be distinguished well due to these three genome sequences were highly homologous [38] (Fig. S8). Fortunately, with the aid of the CRISPR/Cas12a system, we could effectively distinguish SARS-CoV-2 from these two viruses and other respiratory viruses, such as MERS-CoV, hCoV-229E, RSV-A, RSV-B, IVA, and IVB (Fig. 4d). The entire process of using the Hand-CRISPR platform to detect SARS-CoV-2 clinical samples was shown in Fig. 4e, and the overall turnaround time was less than 1 h.

Furthermore, we applied the platform to detect 20 clinical nasopharyngeal swab RNA samples of SARS-CoV-2, provided by the Center for Disease Control and Prevention, Hubei Province, China. We first tested these 20 RNA samples using a clinically approved RT-qPCR kit for SARS-CoV-2. The RT-qPCR results showed that 12 samples were positive and another 8 samples were negative with simultaneous Orf1ab gene and N gene analyses (Fig. S9). Meanwhile, our platform results based on direct observation or UV–vis analysis showed that the detection results of the N gene were 95% consistent with those of RT-qPCR, while the detection results of the Orf1ab gene were 100% consistent with those of RT-qPCR (Fig. 4f). It is worth noting that No. 13 was a positive sample with Ct values of 23.89 (Orf1ab gene) and 23.02 (N gene). However, the detection results of this platform were positive for the Orf1ab gene and negative for the N gene, so it was judged as a suspected case. According to the clinical discriminant method, in this case, we needed to retest the sample, and the final result of the test was consistent with that of the RT-qPCR (Fig. S10). The false-negative result for sample No. 13 may due to the insufficient thawing time. Since the CT value of sample No. 13 was low, the possibility of missed detection by this method due to low sample concentration could be excluded.

4 Conclusions

In this work, a low-cost, human-powered and instrument-free platform was developed for the visual detection of viruses. This platform effectively improved AuNPs-based colorimetric assays for low-concentration target detection. In addition, the handheld nano-centrifugal device is cost-effective (as low as $0.13 US) and is capable of spinning down six samples simultaneously. By combining the CRISPR/Cas12a system with an isothermal amplification reaction, such as the RPA method, the entire operation process for virus detection can be controlled to less than 1 h. The accurate diagnosis of EBV and SARS-CoV-2 further confirmed the reliability and utility of the Hand-CRISPR platform. A comparison of the Hand-CRISPR platform with the other AuNPs-based colorimetric detection platforms provides further evidence of the improvements of this platform (Table S2). In future, the handheld nano-centrifugal device is expected to combine nucleic acid extraction for constructing a full-featured nucleic acids detection system. Besides, we can also combine simpler sample processing methods, such as HUDSON (heating unextracted diagnostic samples to obliterate nucleases) [39], S-PREP (SHERLOCK parasite rapid extraction protocol) [40], PEARL (precipitation-enhanced analyte retrieval) [41], FTA card, etc. Overall, this platform is fully capable of serving as a preliminary screening tool for virus detection in the wild or resource-limited areas and has the potential to shine on the stage of rapid molecular diagnostics.

Supplementary Information The online version contains supplementary material available at https://doi.org/10.1007/s41664-022-00232-0.

Acknowledgements This work was supported by the National Natural Science Foundation of China (91959128, 21874049, 81772246), the Special Project of Science and Technology Development of Guangdong Province (2017B020207011), the Key Research and Development Plan of Hubei Province (2020BCA090), and the Open Funds of the State Key Laboratory of Electroanalytical Chemistry (SKLEAC202001).

Declarations

Conflict of Interest The authors have declared no conflict of interest.

Informed Consent and Ethical Approval The use of clinical SARS-CoV-2 RNA samples for the current study was approved by the ethics committee of the Hubei Provincial Center for Disease Control and Prevention/Academy of Preventive Medicine (2020–061-01). To ensure the safety of patient privacy, waivers of the patients' informed consent were approved by the ethics committee.

References

1. Craw P, Balachandran W. Isothermal nucleic acid amplification technologies for point-of-care diagnostics: a critical review. Lab Chip. 2012;12(14):2469–86.
2. Korf BR, Rehm HL. New approaches to molecular diagnosis. JAMA. 2013;309(14):1511–21.
3. Chertow DS. Next-generation diagnostics with CRISPR. Science. 2018;360(6387):381–2.
4. Li Y, Li S, Wang J, Liu G. CRISPR/Cas systems towards next-generation biosensing. Trends Biotechnol. 2019;37(7): 730–43.
5. Kellner MJ, Koob JG, Gootenberg JS, Abudayyeh OO, Zhang F. SHERLOCK: nucleic acid detection with CRISPR nucleases. Nat Protoc. 2019;14(10):2986–3012.
6. Kilic T, Weissleder R, Lee H. Molecular and immunological diagnostic tests of COVID-19: current status and challenges. iScience. 2020;23(8):101406.
7. Kosack CS, Page AL, Klatser PR. A guide to aid the selection of diagnostic tests. Bull World Health Organ. 2017;95(9):639–45.
8. Elghanian R, Storhoff JJ, Mucic RC, Letsinger RL, Mirkin CA. Selective colorimetric detection of polynucleotides based on the distance-dependent optical properties of gold nanoparticles. Science. 1997;277(5329):1078–81.
9. Li Y, Mansour H, Wang T, Poojari S, Li F. Naked-eye detection of grapevine red-blotch viral infection using a plasmonic CRISPR Cas12a assay. Anal Chem. 2019;91(18):11510–3.
10. Yuan C, Tian T, Sun J, Hu M, Wang X, Xiong E, Cheng M, Bao Y, Lin W, Jiang J, Yang C, Chen Q, Zhang H, Wang H, Wang X, Deng X, Liao X, Liu Y, Wang Z, Zhang G, Zhou X. Universal and naked-eye gene detection platform based on the clustered regularly interspaced short palindromic repeats/Cas12a/13a system. Anal Chem. 2020;92(5):4029–37.
11. Ma L, Peng L, Yin L, Liu G, Man S. CRISPR-Cas12a-Powered Dual-Mode Biosensor for Ultrasensitive and Cross-validating Detection of Pathogenic Bacteria. ACS Sens. 2021;6(8):2920–7.
12. Wong AP, Gupta M, Shevkoplyas SS, Whitesides GM. Egg beater as centrifuge: isolating human blood plasma from whole blood in resource-poor settings. Lab Chip. 2008;8(12):2032–7.
13. Brown J, Theis L, Kerr L, Zakhidova N, O'Connor K, Uthman M, Oden ZM, Richards-Kortum R. A hand-powered, portable, low-cost centrifuge for diagnosing anemia in low-resource settings. Am J Trop Med Hyg. 2011;85(2):327–32.
14. Bhamla MS, Benson B, Chai C, Katsikis G, Johri A, Prakash M. Hand-powered ultralow-cost paper centrifuge. Nat Biomed Eng. 2017;1(1):0009.
15. Byagathvalli G, Pomerantz A, Sinha S, Standeven J, Bhamla MS. A 3D-printed hand-powered centrifuge for molecular biology. PLoS Biol. 2019;17(5): e3000251.
16. Liu CH, Chen CA, Chen SJ, Tsai TT, Chu CC, Chang CC, Chen CF. Blood plasma separation using a fidget-spinner. Anal Chem. 2019;91(2):1247–53.
17. Michael I, Kim D, Gulenko O, Kumar S, Kumar S, Clara J, Ki DY, Park J, Jeong HY, Kim TS, Kwon S, Cho YK. A fidget spinner for the point-of-care diagnosis of urinary tract infection. Nat Biomed Eng. 2020;4(6):591–600.
18. Bohr J, Olsen K. The ancient art of laying rope. Epl Europhys Lett. 2011;93(6004):1–5.
19. Hu M, Yuan C, Tian T, Wang X, Sun J, Xiong E, Zhou X. Single-step, salt-aging-free, and thiol-free freezing construction of AuNP-based bioprobes for advancing CRISPR-based diagnostics. J Am Chem Soc. 2020;142(16):7506–13.
20. Pei H, Li F, Wan Y, Wei M, Liu H, Su Y, Chen N, Huang Q, Fan C. Designed diblock oligonucleotide for the synthesis of spatially isolated and highly hybridizable functionalization of DNA-gold nanoparticle nanoconjugates. J Am Chem Soc. 2012;134(29):11876–9.
21. Niedobitek G, Meru N, Delecluse HJ. Epstein-Barr virus infection and human malignancies. Int J Exp Pathol. 2001;82(3):149–70.
22. Lo YM. Quantitative analysis of Epstein-Barr virus DNA in plasma and serum: applications to tumor detection and monitoring. Ann N Y Acad Sci. 2001;945:68–72.
23. Chan KCA, Woo JKS, King A, Zee BCY, Lam WKJ, Chan SL, Chu SWI, Mak C, Tse IOL, Leung SYM, Chan G, Hui EP, Ma BBY, Chiu RWK, Leung SF, van Hasselt AC, Chan ATC, Lo YMD. Analysis of plasma Epstein-Barr virus DNA to screen for nasopharyngeal cancer. N Engl J Med. 2017;377(6):513–22.
24. Bohn MK, Higgins V, Kavsak P, Hoffman B, Adeli K. High-sensitivity generation 5 cardiac troponin T sex- and age-specific 99th percentiles in the CALIPER cohort of healthy children and adolescents. Clin Chem. 2019;65(4):589–91.
25. Yuan T, Mukama O, Li Z, Chen W, Zhang Y, de Dieu Habimana J, Zhang Y, Zeng R, Nie C, He Z, Zeng L. A rapid and sensitive CRISPR/Cas12a based lateral flow biosensor for the detection of Epstein-Barr virus. Analyst. 2020;145(19):6388–94.
26. Wu X, Tay JK, Goh CK, Chan C, Lee YH, Springs SL, Wang Y, Loh KS, Lu TK, Yu H. Digital CRISPR-based method for the rapid detection and absolute quantification of nucleic acids. Biomaterials. 2021;274: 120876.
27. Yue H, Shu B, Tian T, Xiong E, Huang M, Zhu D, Sun J, Liu Q, Wang S, Li Y, Zhou X. Droplet Cas12a assay enables DNA quantification from unamplified samples at the single-molecule level. Nano Lett. 2021;21(11):4643–53.
28. Vogels CBF, Brito AF, Wyllie AL, Fauver JR, Ott IM, Kalinich CC, Petrone ME, Casanovas-Massana A, Catherine Muenker M, Moore AJ, Klein J, Lu P, Lu-Culligan A, Jiang X, Kim DJ, Kudo E, Mao T, Moriyama M, Oh JE, Park A, Silva J, Song E, Takahashi T, Taura M, Tokuyama M, Venkataraman A, Weizman OE, Wong P, Yang Y, Cheemarla NR, White EB, Lapidus S, Earnest R, Geng B, Vijayakumar P, Odio C, Fournier J, Bermejo S, Farhadian S, Dela Cruz CS, Iwasaki A, Ko AI, Landry ML, Foxman EF, Grubaugh ND. Analytical sensitivity and efficiency comparisons of SARS-CoV-2 RT-qPCR primer-probe sets. Nat Microbiol. 2020;5(10):1299–305.
29. Udugama B, Kadhiresan P, Kozlowski HN, Malekjahani A, Osborne M, Li VYC, Chen H, Mubareka S, Gubbay JB, Chan WCW. Diagnosing COVID-19: the disease and tools for detection. ACS Nano. 2020;14(4):3822–35.

30. Patchsung M, Jantarug K, Pattama A, Aphicho K, Suraritdechachai S, Meesawat P, Sappakhaw K, Leelahakorn N, Ruenkam T, Wongsatit T, Athipanyasilp N, Eiamthong B, Lakkanasirorat B, Phoodokmai T, Niljianskul N, Pakotiprapha D, Chanarat S, Homchan A, Tinikul R, Kamutira P, Phiwkaow K, Soithongcharoen S, Kantiwiriyawanitch C, Pongsupasa V, Trisrivirat D, Jaroensuk J, Wongnate T, Maenpuen S, Chaiyen P, Kamnerdnakta S, Swangsri J, Chuthapisith S, Sirivatanauksorn Y, Chaimayo C, Sutthent R, Kantakamalakul W, Joung J, Ladha A, Jin X, Gootenberg JS, Abudayyeh OO, Zhang F, Horthongkham N, Uttamapinant C. Clinical validation of a Cas13-based assay for the detection of SARS-CoV-2 RNA. Nat Biomed Eng. 2020;4(12):1140–9.
31. Jiang Y, Hu M, Liu AA, Lin Y, Liu L, Yu B, Zhou X, Pang DW. Detection of SARS-CoV-2 by CRISPR/Cas12a-enhanced colorimetry. ACS Sens. 2021;6(3):1086–93.
32. Tian T, Shu B, Jiang Y, Ye M, Liu L, Guo Z, Han Z, Wang Z, Zhou X. An ultralocalized Cas13a assay enables universal and nucleic acid amplification-free single-molecule RNA diagnostics. ACS Nano. 2021;15(1):1167–78.
33. Xiong E, Jiang L, Tian T, Hu M, Yue H, Huang M, Lin W, Jiang Y, Zhu D, Zhou X. Simultaneous dual-gene diagnosis of SARS-CoV-2 based on CRISPR/Cas9-mediated lateral flow assay. Angew Chem Int Ed Engl. 2021;60(10):5307–15.
34. Song Q, Sun X, Dai Z, Gao Y, Gong X, Zhou B, Wu J, Wen W. Point-of-care testing detection methods for COVID-19. Lab Chip. 2021;21(9):1634–60.
35. Feng W, Newbigging AM, Le C, Pang B, Peng H, Cao Y, Wu J, Abbas G, Song J, Wang DB, Cui M, Tao J, Tyrrell DL, Zhang XE, Zhang H, Le XC. Molecular diagnosis of COVID-19: challenges and research needs. Anal Chem. 2020;92(15):10196–209.
36. Kim D, Lee JY, Yang JS, Kim JW, Kim VN, Chang H. The architecture of SARS-CoV-2 transcriptome. Cell. 2020;181(4):914-921e10.
37. Broughton JP, Deng X, Yu G, Fasching CL, Servellita V, Singh J, Miao X, Streithorst JA, Granados A, Sotomayor-Gonzalez A, Zorn K, Gopez A, Hsu E, Gu W, Miller S, Pan CY, Guevara H, Wadford DA, Chen JS, Chiu CY. CRISPR-Cas12-based detection of SARS-CoV-2. Nat Biotechnol. 2020;38(7):870–4.
38. Rangan R, Zheludev IN, Hagey RJ, Pham EA, Wayment-Steele HK, Glenn JS, Das R. RNA genome conservation and secondary structure in SARS-CoV-2 and SARS related viruses: a first look. RNA. 2020;26:937–59.
39. Myhrvold C, Freije CA, Gootenberg JS, Abudayyeh OO, Metsky HC, Durbin AF, Kellner MJ, Tan AL, Paul LM, Parham LA, Garcia KF, Barnes KG, Chak B, Mondini A, Nogueira ML, Isern S, Michael SF, Lorenzana I, Yozwiak NL, MacInnis BL, Bosch I, Gehrke L, Zhang F, Sabeti PC. Field-deployable viral diagnostics using CRISPR-Cas13. Science. 2018;360(6387):444–8.
40. Lee RA, Puig H, Nguyen PQ, Angenent-Mari NM, Donghia NM, McGee JP, Dvorin JD, Klapperich CM, Pollock NR, Collins JJ. Ultrasensitive CRISPR-based diagnostic for field-applicable detection of Plasmodium species in symptomatic and asymptomatic malaria. Proc Natl Acad Sci USA. 2020;117(41):25722–31.
41. Rauch JN, Valois E, Solley SC, Braig F, Lach RS, Audouard M, Ponce-Rojas JC, Costello MS, Baxter NJ, Kosik KS, Arias C, Acosta-Alvear D, Wilson MZ. A scalable, easy-to-deploy protocol for Cas13-based detection of SARS-CoV-2 genetic material. J Clin Microbiol. 2021;59(4):1–9.